ACS Photonics

Article

pubs.acs.org/journal/apchd5

Enhanced Outcoupling in Organic Light-Emitting Diodes via a High-Index Contrast Scattering Layer

Tae-Wook Koh,[*,†,⊥] Joshua A. Spechler,[‡,§,⊥] Kyung Min Lee,[†] Craig B. Arnold,[†,‡,§] and Barry P. Rand[*,†,§,∥]

[†]Department of Electrical Engineering, [‡]Department of Mechanical and Aerospace Engineering, [§]Princeton Institute for the Science and Technology of Materials (PRISM), and [∥]Andlinger Center for Energy and the Environment, Princeton University, Princeton, New Jersey 08544, United States

Supporting Information

ABSTRACT: Despite high internal quantum efficiencies, planar organic light-emitting diodes (OLEDs) typically suffer from limited outcoupling efficiencies. To improve this outcoupling efficiency, we have developed a new thin (~2 μm) light scattering layer that employs air voids (low-index scattering centers) embedded in a high-index polyimide matrix to effectively frustrate the substrate-trapped light, increasing the outcoupling efficiency. The porous polyimide scattering layers are created through the simple and scalable fabrication technique of phase inversion. The optical properties of the scattering layers have been characterized via microscopy, transmittance/haze measurements, and ellipsometry, which demonstrate the excellent scattering properties of these layers. We have integrated these films into a green OLED stack, where they show a 65% enhancement of the external quantum efficiency and a 77% enhancement of the power efficiency. Furthermore, we have integrated these layers into a white OLED and observed similar enhancements. Both the green and white OLEDs additionally demonstrate excellent color stability over wide viewing angles with the integration of this thin scattering layer.

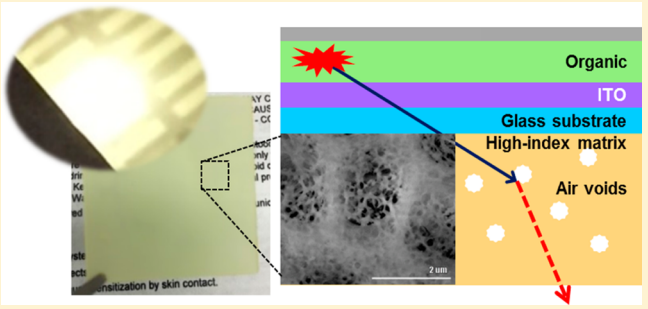

KEYWORDS: *organic light-emitting diodes (OLEDs), phase inversion, outcoupling efficiency, scattering layer*

Since the first observation of electroluminescence in organic solids[1] and the demonstration of a bilayer fluorescent organic light-emitting diode (OLED),[2] significant improvements have been realized in this thin-film-based photonic device. The development of materials with improved transport properties,[3,4] chemical and thermal stabilities,[5,6] and high luminescence quantum yields[7,8] has resulted in several important breakthroughs in device performance, while a deeper understanding of the device physics and interfacial properties[9−11] has allowed engineering devices to realize internal quantum efficiencies near the theoretical maximum of 100%.[12,13] While the device electrical efficiency is approaching its limit, there is still significant room for improvement in the optical efficiency, often called the outcoupling efficiency or light extraction efficiency. Outcoupling efficiency can be calculated with the aid of advanced modeling techniques,[14−16] which show that only approximately 20−30% of the emitted photons escape a noncavity planar OLED fabricated on a conventional glass substrate.[17−19] Hence, in order to fully convert the input electrical power into optical power, it is essential to overcome this low outcoupling efficiency.

It should be noted that two factors are closely associated with the typically low OLED outcoupling efficiency: the planarity of the device and the refractive indices of the thin-film stack. A planar organic−metal interface leads to evanescently coupled surface plasmonic losses,[20] while an index gradient starting from high-index organic layers to a mid-index glass substrate to low-index ambient air leads to laterally traveling waveguided and substrate-trapped loss modes.[21] While the surface plasmonic loss mode can be reduced by spacing oscillating dipoles (i.e., emitters) away from the organic−metal interface or by introducing corrugation,[22] recovery of waveguided and substrate-trapped losses in bottom-emitting OLEDs requires modifications of the optical structure. One efficient way to deal with these two loss modes simultaneously is to adopt a high-index substrate that can trade the waveguided mode for a substrate-trapped mode while simultaneously applying an external extraction structure such as a pyramidal[23] or microlens array.[24] However, fabrication of these structures involves numerous processing steps and does not lend itself toward low-cost upscaling. An alternative approach is to use a composite scattering film,[25−28] where the index contrast between the host medium (typically the substrate itself) and high-index nano/microparticles induces scattering that redistributes the direction of light propagation. Though this approach has been successful in improving the outcoupling efficiency, it contradicts the desire for a high-index substrate

Received: June 23, 2015
Published: August 13, 2015

DOI: 10.1021/acsphotonics.5b00346
ACS Photonics 2015, 2, 1366−1372

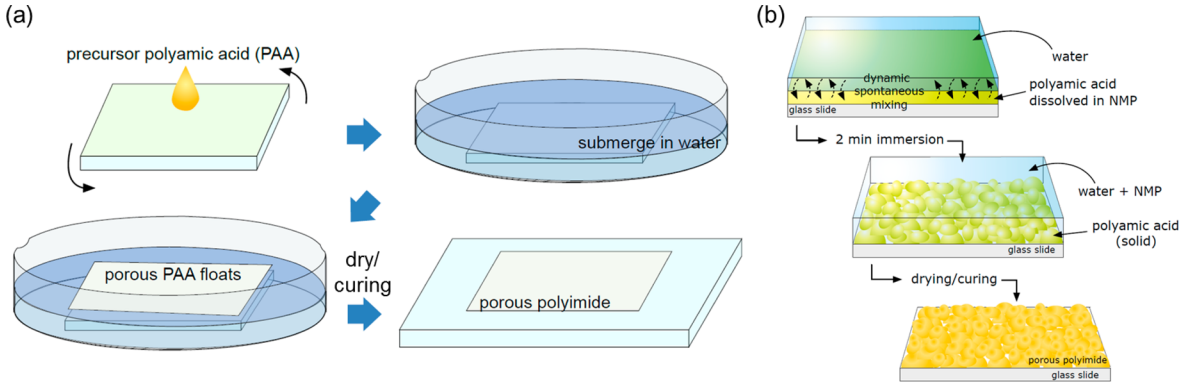

Figure 1. (a) Experimental schematic of the fabrication of a porous polyimide (p-PI) layer. (b) Stepwise illustration of the dynamic formation of porosity inside the p-PI layer.

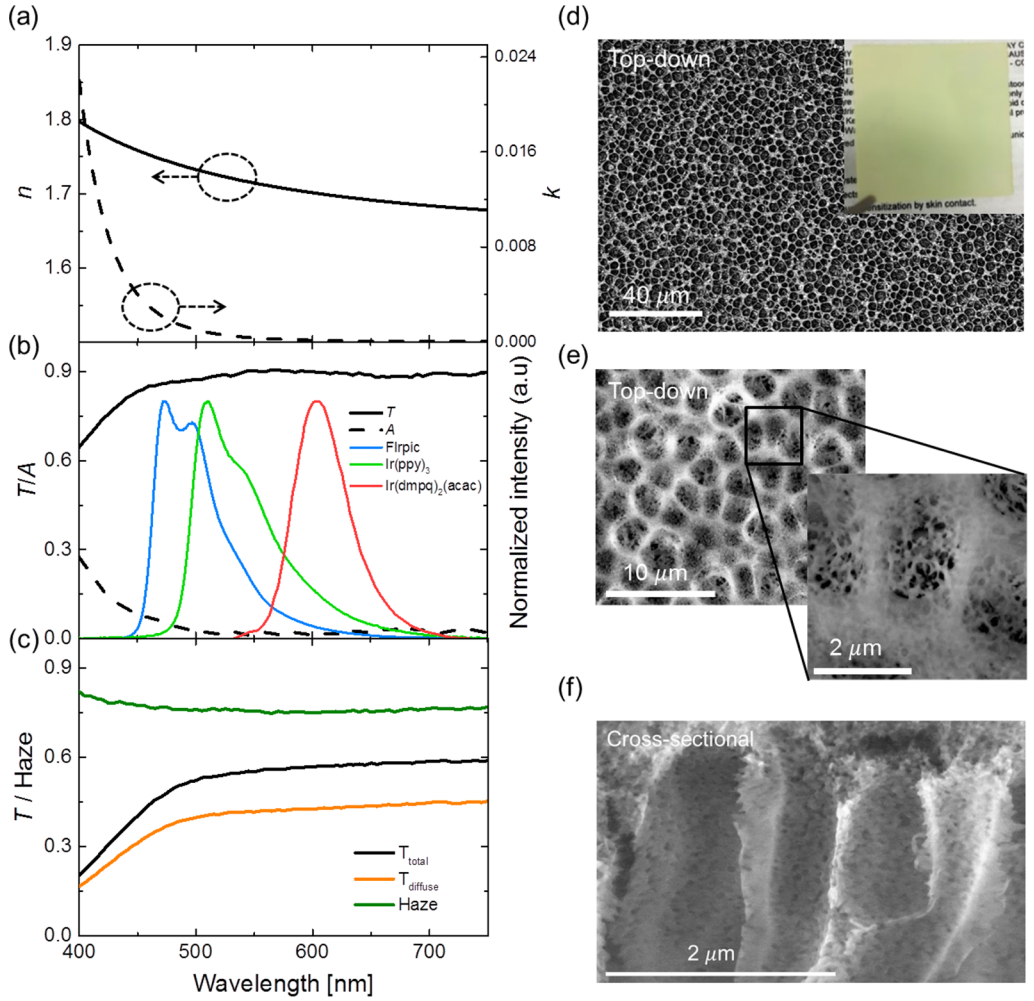

Figure 2. (a) Refractive index (n) and extinction coefficient (k) of the polyimide used in this work. (b) Transmission (T) and absorption (A) spectra of an 870 nm thick plain polyimide film and the intrinsic photoluminescence spectra of blue (FIrpic), green ($Ir(ppy)_3$), and red ($Ir(dmpq)_2(acac)$) phosphorescent dopants for the OLEDs employed in this work. (c) Measured total and diffuse transmission and calculated haze spectra for the p-PI scattering layer. (d) Top-down confocal microscopy image (the inset is a photograph of the p-PI layer on a glass substrate), (e) top-down SEM image, and (f) cross-sectional SEM image of the p-PI scattering layer.

and host medium: that is, as the index of the substrate/host medium gets higher, the smaller the index contrast between the host medium and scattering particles becomes, leading to a less effective scattering-induced outcoupling efficiency enhancement.

Here we demonstrate a simple yet effective method of fabricating flexible polymeric scattering layers for OLEDs that requires no costly patterning, etching, or molding processes, aspects that are desirable for mass production of large-scale lighting panels. The chosen process is that of phase inversion or, more specifically, immersion precipitation, which is widely

DOI: 10.1021/acsphotonics.5b00346
ACS Photonics 2015, 2, 1366−1372

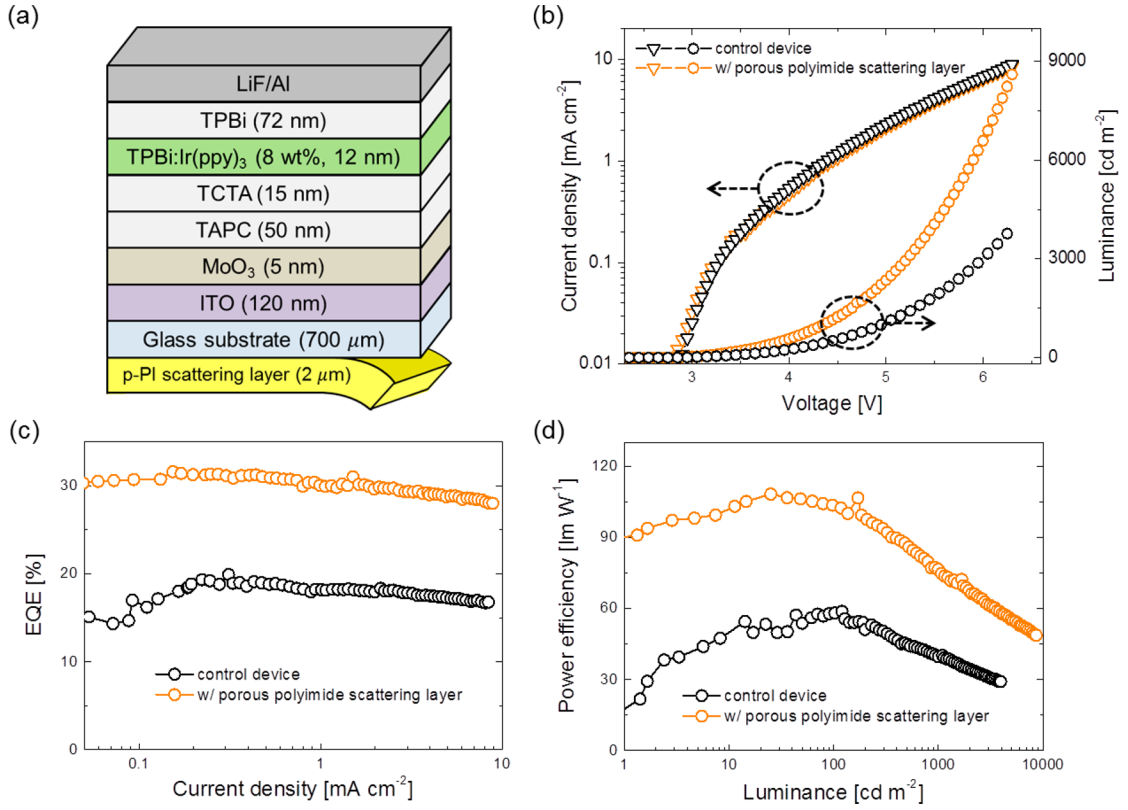

Figure 3. (a) Device structures of the green phosphorescent OLEDs with and without a p-PI scattering layer. (b) Current density−luminance−voltage (J−L−V) curves for the OLEDs. (c) External quantum efficiency (EQE) vs J curves and (d) power efficiency vs L curves for OLEDs with and without a p-PI scattering layer.

used in the preparation of polymeric membranes for filter applications.[29] By using this technique, we have fabricated high-index polyimide films embedded with air voids. The large index contrast between the polyimide film and air void scattering sites results in an effective platform to ensure effective scattering and outcoupling of waveguided light. The polyimide has a refractive index (n) greater than 1.7 and negligible absorption at wavelengths (λ) greater than 460 nm, making it a good candidate for the host medium of a scattering layer.

RESULTS AND DISCUSSION

Figure 1a shows the fabrication scheme of our porous polyimide (p-PI) films using the scalable phase inversion technique. We begin by spin-coating a film of the polymer/solvent solution of interest. This film is then immersed in an antisolvent that does not dissolve the polymer but is miscible with the first solvent. The result of this process is a porous polymer structure. Figure 1b illustrates the dynamic formation of air voids within the precursor polyamic acid films. In short, the physics of immersion precipitation relies on the interaction between a solution and an antisolvent, a liquid that does not dissolve the solid material in the solution. Furthermore, the antisolvent must be miscible with the solution solvent. Upon immersion of the solution in an antisolvent bath the solid violently coagulates, and under the right choice of solution and antisolvent this coagulated film can create a nanoporous structure.[30,31] Previous work has characterized the use of specific solvents and antisolvents for polyimide precursor polyamic acid (PAA) solutions.[32,33] In this work, the PAA is dissolved in a polar aprotic solvent, *N*-methyl-2-pyrrolidone (NMP). Water serves as a suitable and scalable antisolvent for this system. The phase inversion PAA layer has a hazy appearance that persists even after the thermal imidization step that converts the film into the p-PI film. While other studies have reported the need to maintain contact between the solvent and antisolvent for as long as 24 h, our devices require only thin films of p-PI (~2 μm), which coagulate quickly and allow us to complete the process with only 2 min of immersion time.[34] The lamination of the PAA films to the glass substrates does not require any additional surface treatment or adhesive, and after the thermal imidization process the adhesion between the p-PI film and the glass substrate is highly robust. Sonication of the substrates in a hot (60 °C) bath of water, acetone, or isopropanol had no effect on the p-PI film structure or the adhesion between the film and the glass.

The optical characterization of the polyimide is summarized in Figure 2a−c. Refractive indices measured on a film via ellipsometry are shown in Figure 2a. The index and extinction coefficient are n = 1.74 and k = 0.002, respectively, at λ = 475 nm, the emission peak for the blue phosphorescent emitter FIrpic, and 1.73 and 0.0008 at λ = 510 nm, the emission peak for the green phosphorescent emitter Ir(ppy)$_3$. The refractive indices at these two representative wavelengths are indeed high enough to concentrate the optical power to the scattering layer, while k values are small enough to justify the use of this polyimide as the host medium without significant parasitic absorption. This is also clear from the measured transmission (T) and absorption (A) spectra of an 870 nm thick plain polyimide film (fabricated using the same spin-coating conditions as the porous version) shown in Figure 2b, plotted together with the intrinsic photoluminescence spectra of the blue (FIrpic), green (Ir(ppy)$_3$), and red (Ir(dmpq)$_2$(acac))

DOI: 10.1021/acsphotonics.5b00346
ACS Photonics 2015, 2, 1366−1372

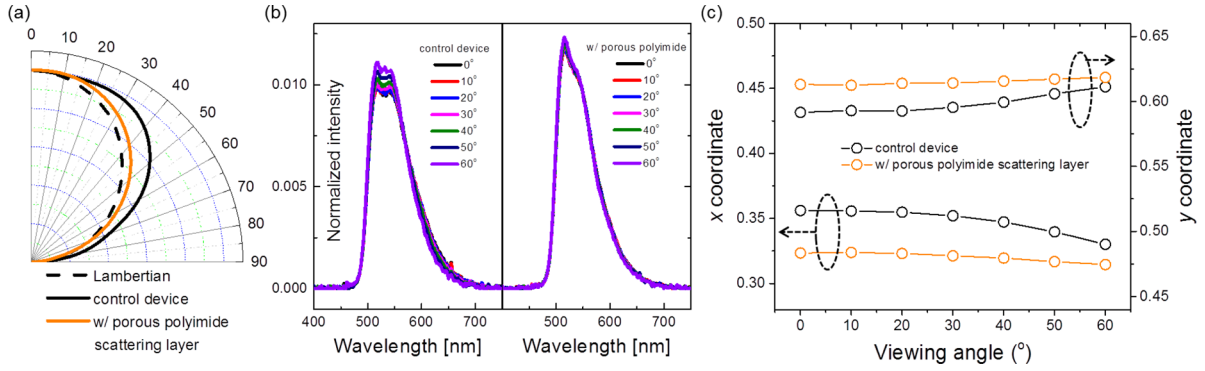

Figure 4. (a) Angular emission intensity profiles of green OLEDs normalized to the emission at the substrate normal. The dashed curve shows a Lambertian profile. (b) Electroluminescence spectra and (c) CIE *x* and *y* coordinates of OLEDs with and without the p-PI scattering layer measured at viewing angles from 0° (substrate normal) to 60°.

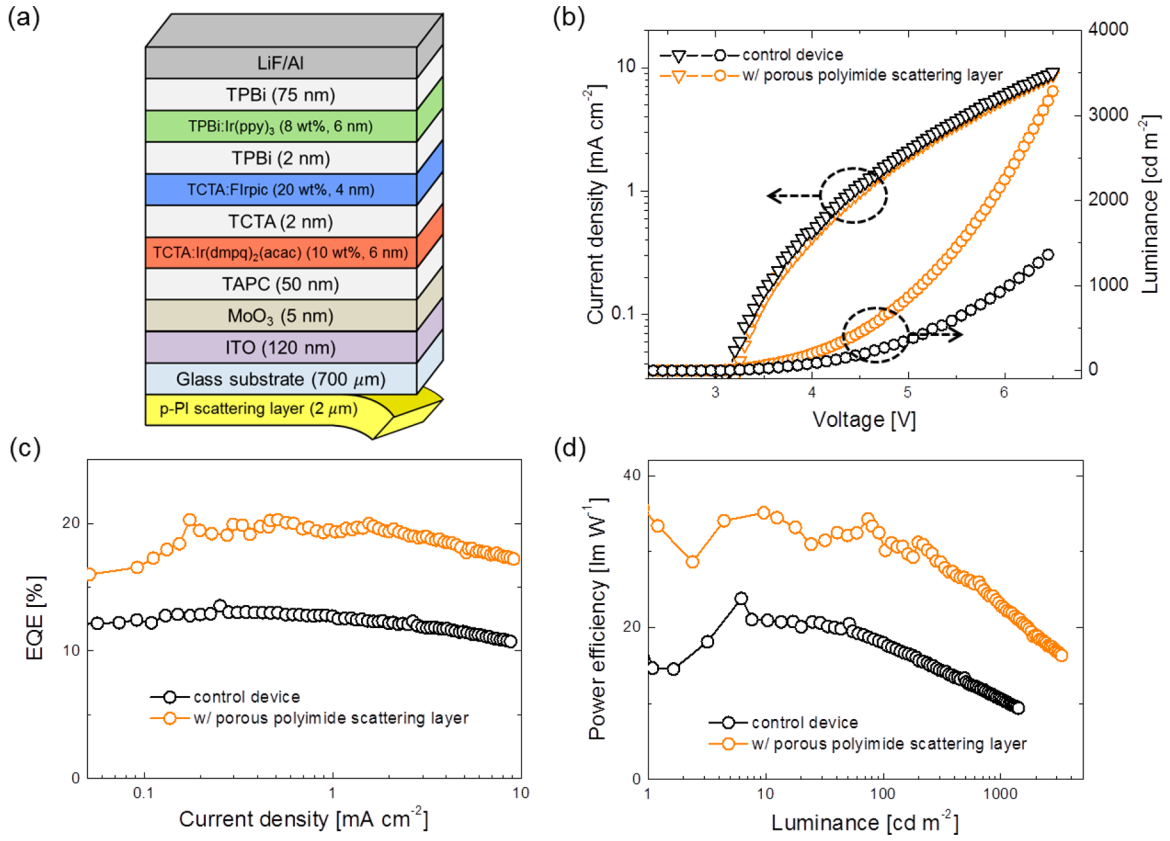

Figure 5. (a) Device structures of WOLEDs with and without a p-PI layer on the back of the glass/ITO substrate. (b) Current density–luminance–voltage (*J*–*L*–*V*) characteristics of the WOLEDs. (c) External quantum efficiency (EQE) vs *J* curves and (d) power efficiency vs luminance curves for WOLEDs with and without a p-PI scattering layer.

phosphorescent emitters used in this work to construct a prototypical white OLED (WOLED).

We further characterized the p-PI layers via haze measurements and microscopy, as shown in Figure 2c–f (the Figure 2d inset shows a photograph of the p-PI film on glass). The confocal microscopy image (Figure 2d) reveals a highly porous framework characterized by voids of a few microns in extent. The structure is hierarchical in nature, consisting of nanoscale voids that are clearly visible in the scanning electron microscopy (SEM) images (Figure 2e,f). The haze of the film is confirmed qualitatively in the photograph shown in the Figure 2d inset and quantitatively in the haze data presented in Figure 2c. Indeed, most of the transmission through the scattering film is diffuse, leading to an average haze of 77% in the visible wavelength range as summarized. Throughout this work, we utilized a 2 μm thick p-PI layer.

To verify their ability to enhance the optical outcoupling efficiency in OLEDs, we integrated the p-PI films on the backside of glass/indium tin oxide (ITO) substrates, as shown in the device schematic in Figure 3a. A 5 nm MoO_3 layer was used as a hole injection layer to inject holes into the 50 nm thick TAPC and 15 nm thick TCTA hole transport layers. TPBi was used as both the phosphorescent host layer (12 nm) and the electron transport layer (72 nm), and $Ir(ppy)_3$ was doped into TPBi at 8% by weight. The thicknesses of TAPC hole transport and TPBi electron transport layers were designed to

DOI: 10.1021/acsphotonics.5b00346
ACS Photonics 2015, 2, 1366–1372

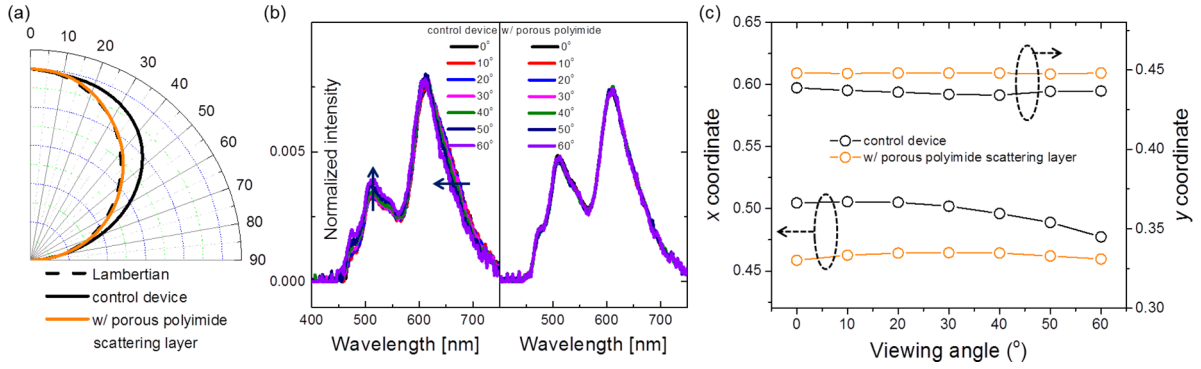

Figure 6. (a) Angular emission intensity profiles of WOLEDs normalized to the emission at the substrate normal. The dashed curve shows a Lambertian emission profile. (b) Electroluminescence spectra and (c) CIE x and y coordinates of WOLEDs without and with the p-PI scattering layer measured at viewing angles from 0° (substrate normal) to 60°.

maximize the sum of the outcoupled and substrate-trapped modes while maintaining a high outcoupled mode portion in the green OLEDs on the basis of a power spectral density theory calculation[17] (Figure S2 in the Supporting Information). The current density−forward luminance−voltage (J−L−V) characteristics are given in Figure 3b, which shows identical J−V but different L−V graphs for OLEDs with and without the p-PI layer, as expected since the modification is external. Plots of the external quantum efficiency (EQE) versus J and the power efficiency (PE) versus L are shown in Figure 3c,d, respectively, to give a comprehensive understanding of the outcoupling efficiency of the devices. The EQE at a current density of 1 mA cm^{-2} was 18.2% for the control device and increased to 30.0%, an enhancement of 65%, after the p-PI scattering layer was applied to the substrate backside. The PE was measured to be 58.5 lm W^{-1} for the control device at a forward luminance of 100 cd m^{-2}, which increased to 103.6 lm W^{-1} with the aid of the p-PI layer. This enhancement ratio of 77% for the power efficiency is higher than that for the EQE simply because the same forward luminance is reached at a lower driving voltage and thus a lower driving current for the p-PI-layer-assisted device.

Normalized angular emission intensity profiles, normalized electroluminescence (EL) spectra, and Commission International de l'Eclairage (CIE) 1931 chromaticity coordinates at different viewing angles are provided in Figure 4. Even though the ITO electrode has a relatively high transmittance and low reflectance, there is nevertheless a weak microcavity effect,[35] as evidenced by the fact that the angular intensity profile is slightly wider than Lambertian. Additionally, there is a slight increase in the height of the dominant emission peak of $Ir(ppy)_3$ together with a narrowing of the long-wavelength tail as a function of viewing angle. After application of the p-PI scattering layer, the angular intensity adopts a nearly Lambertian profile. This is the case because the p-PI layer redistributes the light propagation randomly, leading to a considerably more uniform spectral distribution across the entire forward hemisphere, as shown in Figure 4b. Furthermore, as shown in Figure 4c, the CIE 1931 (x, y) coordinates (the color diagram is available in Figure S3) of the control device are (0.356, 0.592) at 0° (substrate normal) and (0.330, 0.611) at 60° with a $|\Delta(x, y)|$ of (0.026, 0.019), while those of the device with a p-PI scattering layer attached to it are (0.323, 0.613) at 0° and (0.315, 0.618) at 60° with a significantly smaller $|\Delta(x, y)|$ of (0.008, 0.005).

On the basis of the enhancements observed for green OLEDs with the p-PI layer, we also demonstrated WOLEDs to prove the effectiveness of our approach for a broadband emission spectrum. The WOLED device structure, J−L−V graphs, and EQE−J and PE−L plots are shown in Figure 5. The phosphorescent dopants $Ir(dmpq)_2(acac)$, FIrpic, and $Ir(ppy)_3$ were used as red, blue, and green emitters, respectively. In this structure, excitons are generated in the TCTA and TPBi hosts within the vicinity of the TCTA−TPBi interface to be utilized directly on FIrpic molecules or diffused away from the interface to generate red and green emission, as has been described previously.[36] A 50 nm thick TAPC layer and a 75 nm thick TPBi layer are used as the hole transport and electron transport layers, respectively. The glass/ITO control device had an EQE of 11.9% at a current density of 3 mA cm^{-2}, and the p-PI-layer-assisted device showed an increased EQE of 19.0% at the same current density, corresponding to a 60% enhancement of the optical outcoupling efficiency. This enhancement ratio is similar to that in the previous case of the green OLED, confirming that the absorption loss within the p-PI layer is negligible while the scattering mechanism operates equally well across the broadband white spectrum. The PE at a forward luminance of 100 cd m^{-2} was 18.0 lm W^{-1} for the control device, whereas it increased to 32.1 lm W^{-1} for the p-PI assisted device, corresponding to a 78% enhancement.

The angular emission intensity profile, EL spectra, and CIE 1931 coordinates of the WOLEDs are displayed in Figure 6. The angular intensity profile was initially broader than Lambertian for the control WOLED and was similarly narrowed upon application of the p-PI layer (Figure 6a), and the EL spectra at different viewing angles overlap identically (Figure 6b). The color consistency across the viewing angle range improved considerably. The CIE (x, y) coordinates of the control WOLED (the color diagram is available in Figure S3, and a photograph of a working WOLED is shown in Figure S4) are (0.505, 0.439) at 0° and (0.477, 0.437) at 60° with a $|\Delta(x, y)|$ of (0.028, 0.002), while for the WOLED with a p-PI layer they are (0.462, 0.448) at 0° and (0.461, 0.448) at 60° with a notably small $|\Delta(x, y)|$ of (0.001, 0.000), which is ideal for lighting applications.

To understand the balance of photon density within the thin-film OLED structure and be able to determine the potential gains from a scattering-based outcoupling approach, we calculated the portions of each loss and outcoupled mode in the case of a green phosphorescent OLED with the same optical simulation code as used for Figure S2. This calculation provides relative portions of outcoupled, substrate-trapped, waveguided, and surface plasmonic loss modes for a given

DOI: 10.1021/acsphotonics.5b00346
ACS Photonics 2015, 2, 1366−1372

device structure and power spectral dissipation density with respect to the in-plane wavevector at wavelengths of interest. The power spectral dissipation density at a representative wavelength of λ = 510 nm (the emission peak of $Ir(ppy)_3$) is plotted in Figure S5. This power dissipation density was integrated over the designated in-plane wavevector ranges, and the results are summarized in Table 1, which shows the relative

Table 1. Relative Portions of the Outcoupled Mode and Energy Loss Modes in a Green Phosphorescent OLED Calculated Using a Power Spectral Dissipation Density Model[17]

outcoupled	absorption	waveguided	surface plasmonic	substrate-trapped
21.1%	4.6%	15.6%	27.2%	31.5%

portion of each mode in the device assuming a 100% internal quantum yield. From the calculated portions of the loss modes, we speculate that our p-PI scattering layer effectively recovered almost half (44%) of the substrate-trapped mode, enabling a 65% enhancement in the outcoupled mode. Furthermore, through the introduction of a thicker doped transport layer to minimize the surface plasmonic loss without compromising the electrical efficiency[16] and a high-index substrate to maximize the substrate-trapped mode, our high-index scattering layer with air void scattering centers can be further optimized for outcoupling efficiency.

CONCLUSION

In conclusion, we have employed the process of phase inversion as a straightforward, scalable, and low-cost technique to fabricate flexible polymeric scattering layers. With polyimide as a high-index host medium and air voids as scattering centers, porous polyimide (p-PI) layers applied to green and broadband OLEDs show outcoupling efficiency enhancements of 65% and 60%, respectively. These enhancements are achievable because of the large refractive index difference (>0.7) between the high-index polyimide host medium and the low-index air voids as well as the fact that the index of polyimide is greater than that of the glass substrate, which is beneficial for extracting substrate-trapped light into the scattering layer. In addition to the enhanced outcoupling efficiency, excellent color consistency between viewing angles of 0° and 60° is also confirmed via a small $|\Delta(x, y)|$ shift of (0.001, 0.000) for the WOLED. An optical simulation based on power spectral density theory suggests that utilizing a substrate with a higher index compared with glass would lead to conversion of the waveguided mode into the substrate-trapped mode, which could be readily recovered by the proposed high-index scattering layer. In view of the fact that high-index glass substrates are considerably more expensive than conventional substrates, WOLEDs on flexible, high-index plastic substrates with a scattering layer prepared by phase inversion can be an effective outcoupling enhancement strategy for future lighting applications.

METHODS

Porous Polyimide Scattering Layer Fabrication and Characterization. The PAA precursor (liquid PI2525, HD Microsystems) dissolved in NMP (Sigma-Aldrich) was spun onto a glass microscope slide at 1000 rpm for 90 s. Then the slide was immersed in a water bath for at least 2 min. The porous, hazy phase inversion PAA film floated to the air−water bath interface. The film was then transferred onto the backside of an ITO-coated substrate. The film was thoroughly dried under vacuum at 50 °C and then cured at 160 and 360 °C each for 20 min in a furnace, which thermally imidized the PAA to create a hazy, porous polyimide layer. An integrating sphere and calibrated Si photodiode (Labsphere) used together with a monochromator (TLS-300X, Newport) was used to measure the total/diffuse transmission, absorption, and haze. Confocal microscopy was performed with an Olympus LEXT scanning laser confocal microscope with a 50× N.A. = 0.95 objective under 405 nm laser illumination. SEM images were obtained with a FEI Quanta environmental scanning electron microscope. Samples were prepared by freezing in liquid nitrogen and then cleavage to obtain an edge-on image. The low-vacuum large-field secondary electron detection mode was used to image the uncoated, nonconductive polyimide. The chamber pressure was set to 0.83 Torr, and the electron beam was accelerated at 10 kV.

Device Fabrication and Analysis. Once the porous polyimide scattering layers were lifted from the bath on the backside of ITO substrates and cross-linked, they remained stable and intact against the physical and chemical cleaning processes. Substrates with patterned ITO electrodes in the front were cleaned using soapy water, deionized water, acetone, and isopropanol in sequence using an ultrasonicator for 20 min each and then treated with O_2 plasma for 5 min. Next, the substrates were brought into a vacuum evaporation chamber (EvoVac, Angstrom Engineering, base pressure $\approx 5 \times 10^{-7}$ Torr) for thermal evaporation of MoO_3 (Alfa Aesar), 4,4′-cyclohexylidenebis[*N*,*N*-bis(4-methylphenyl)benzenamine] (TAPC) (Nichem), 4,4′,4″-tris(9-carbazoyl)triphenylamine (TCTA) (Nichem), and 2,2′,2″-(1,3,5-benzinetriyl)-tris(1-phenyl-1*H*-benzimidazole (TPBi) (Nichem). Tris[2-phenylpyridinato-C^2,*N*]iridium(III) ($Ir(ppy)_3$) (Nichem) was coevaporated with TPBi for the green emissive layer, and bis[2-(4,6-difluorophenyl)pyridinato-C^2,*N*](picolinato)iridium(III) (FIrpic) (Nichem) and bis(2-(3,5-dimethylphenyl)quinoline-C^2,*N*′)(acetylacetonato)iridium(III) ($Ir(dmpq)_2(acac)$) (Nichem) were coevaporated with TCTA at desired doping ratios for blue and red emissive layers, respectively. A LiF/Al cathode contact was used for both the green and white OLEDs with 0.1 cm^2 device area. All of the organic materials were purified using a thermal gradient tube furnace (Lindberg/Blue M, Thermo Scientific) before use. The fabricated devices were measured using a homemade motorized goniometer setup consisting of a Keithley 2400 sourcemeter unit, a calibrated Si photodiode (FDS-100-CAL, Thorlabs), a picoammeter (4140B, Agilent), and a calibrated fiber optic spectrophotometer (UVN-SR, StellarNet Inc.)

ASSOCIATED CONTENT

Supporting Information

The Supporting Information is available free of charge on the ACS Publications website at DOI: 10.1021/acsphotonics.5b00346.

Figures S1−S5 (PDF)

AUTHOR INFORMATION

Corresponding Authors

*E-mail: tkoh@princeton.edu.
*E-mail: brand@princeton.edu.

DOI: 10.1021/acsphotonics.5b00346
ACS Photonics 2015, 2, 1366−1372

Author Contributions

[⊥]T.-W.K. and J.A.S. contributed equally to this work.

Notes

The authors declare no competing financial interest.

■ ACKNOWLEDGMENTS

We acknowledge funding for this work from the DOE EERE SSL Program under Award DE-EE0006672. J.A.S. and C.B.A. acknowledge support from the Rutgers−Princeton NSF IGERT on Nanotechnology for Clean Energy. B.P.R. acknowledges support from a 3M Nontenured Faculty Award.

■ REFERENCES

(1) Helfrich, W.; Schneider, G. Recombination Radiation in Anthracene Crystals. *Phys. Rev. Lett.* **1965**, *14*, 229−231.
(2) Tang, C. W.; VanSlyke, S. A. Organic electroluminescent diodes. *Appl. Phys. Lett.* **1987**, *51*, 913−915.
(3) Murata, H.; Kafafi, Z. H.; Uchida, M. Efficient organic light-emitting diodes with undoped active layers based on silole derivatives. *Appl. Phys. Lett.* **2002**, *80*, 189−191.
(4) Oh, H.-Y.; Lee, C.; Lee, S. Efficient blue organic light-emitting diodes using newly-developed pyrene-based electron transport materials. *Org. Electron.* **2009**, *10*, 163−169.
(5) Tao, Y.; Wang, Q.; Yang, C.; Wang, Q.; Zhang, Z.; Zou, T.; Qin, J.; Ma, D. A Simple Carbazole/Oxadiazole Hybrid Molecule: An Excellent Bipolar Host for Green and Red Phosphorescent OLEDs. *Angew. Chem., Int. Ed.* **2008**, *47*, 8104−8107.
(6) Steuber, F.; Staudigel, J.; Stössel, M.; Simmerer, J.; Winnacker, A.; Spreitzer, H.; Weissörtel, F.; Salbeck, J. White Light Emission from Organic LEDs Utilizing Spiro Compounds with High-Temperature Stability. *Adv. Mater.* **2000**, *12*, 130−133.
(7) Baldo, M. A.; O'Brien, D. F.; You, Y.; Shoustikov, A.; Sibley, S.; Thompson, M. E.; Forrest, S. R. Highly efficient phosphorescent emission from organic electroluminescent devices. *Nature* **1998**, *395*, 151−154.
(8) Ulbricht, C.; Beyer, B.; Friebe, C.; Winter, A.; Schubert, U. S. Recent Developments in the Application of Phosphorescent Iridium(III) Complex Systems. *Adv. Mater.* **2009**, *21*, 4418−4441.
(9) Meyer, J.; Hamwi, S.; Kröger, M.; Kowalsky, W.; Riedl, T.; Kahn, A. Transition Metal Oxides for Organic Electronics: Energetics, Device Physics and Applications. *Adv. Mater.* **2012**, *24*, 5408−5427.
(10) Ma, H.; Yip, H.-L.; Huang, F.; Jen, A. K.-Y. Interface Engineering for Organic Electronics. *Adv. Funct. Mater.* **2010**, *20*, 1371−1388.
(11) Erickson, N. C.; Holmes, R. J. Engineering Efficiency Roll-Off in Organic Light-Emitting Devices. *Adv. Funct. Mater.* **2014**, *24*, 6074−6080.
(12) Kawamura, Y.; Goushi, K.; Brooks, J.; Brown, J. J.; Sasabe, H.; Adachi, C. 100% phosphorescence quantum efficiency of Ir(III) complexes in organic semiconductor films. *Appl. Phys. Lett.* **2005**, *86*, 071104.
(13) Yersin, H. *Highly Efficient OLEDs with Phosphorescent Materials*; Wiley-VCH: Weinheim, Germany, 2008.
(14) Benisty, H.; Stanley, R.; Mayer, M. Method of source terms for dipole emission modification in modes of arbitrary planar structures. *J. Opt. Soc. Am. A* **1998**, *15*, 1192−1201.
(15) Smith, L. H.; Wasey, J. A. E.; Samuel, I. D. W.; Barnes, W. L. Light Out-Coupling Efficiencies of Organic Light-Emitting Diode Structures and the Effect of Photoluminescence Quantum Yield. *Adv. Funct. Mater.* **2005**, *15*, 1839−1844.
(16) Meerheim, R.; Furno, M.; Hofmann, S.; Lüssem, B.; Leo, K. Quantification of energy loss mechanisms in organic light-emitting diodes. *Appl. Phys. Lett.* **2010**, *97*, 253305.
(17) Furno, M.; Meerheim, R.; Hofmann, S.; Lüssem, B.; Leo, K. Efficiency and rate of spontaneous emission in organic electroluminescent devices. *Phys. Rev. B: Condens. Matter Mater. Phys.* **2012**, *85*, 115205.
(18) Kim, S.-Y; Jeong, W.-I.; Mayr, C.; Park, Y.-S.; Kim, K.-H.; Lee, J.-H.; Moon, C.-K.; Brütting, W.; Kim, J.-J. Organic Light-Emitting Diodes with 30% External Quantum Efficiency Based on a Horizontally Oriented Emitter. *Adv. Funct. Mater.* **2013**, *23*, 3896−3900.
(19) Gather, M. C.; Reineke, S. Recent advances in light outcoupling from white organic light-emitting diodes. *J. Photonics Energy* **2015**, *5*, 057607.
(20) Hobson, P. A.; Wedge, S.; Wasey, J. A. E.; Sage, I.; Barnes, W. L. Surface Plasmon Mediated Emission from Organic Light-Emitting Diodes. *Adv. Mater.* **2002**, *14*, 1393−1396.
(21) Sun, Y.; Forrest, S. R. Enhanced light out-coupling of organic light-emitting devices using embedded low-index grids. *Nat. Photonics* **2008**, *2*, 483−487.
(22) Koo, W. H.; Youn, W.; Zhu, P.; Li, X.-H.; Tansu, N.; So, F. Light Extraction of Organic Light Emitting Diodes by Defective Hexagonal-Close-Packed Array. *Adv. Funct. Mater.* **2012**, *22*, 3454−3459.
(23) Chen, M.-L.; Wei, A.-C.; Shieh, H.-P. D. Increased Organic Light-Emitting Diode Panel Light Efficiency by Optimizing Structure and Improving Alignment of Pyramidal Array Light-Enhancing Layers. *Jpn. J. Appl. Phys.* **2007**, *46*, 1521−1525.
(24) Möller, S.; Forrest, S. R. Improved light out-coupling in organic light emitting diodes employing ordered microlens arrays. *J. Appl. Phys.* **2002**, *91*, 3324−3327.
(25) Bathelt, R.; Buchhauser, D.; Gärditz, C.; Paetzold, R.; Wellmann, P. Light extraction from OLEDs for lighting applications through light scattering. *Org. Electron.* **2007**, *8*, 293−299.
(26) Shiang, J. J.; Duggal, A. R. Application of radiative transport theory to light extraction from organic light emitting diodes. *J. Appl. Phys.* **2004**, *95*, 2880−2888.
(27) Liu, R.; Ye, Z.; Park, J.-M.; Cai, M.; Chen, Y.; Ho, K.-M.; Shinar, R.; Shinar, J. Microporous phase-separated films of polymer blends for enhanced outcoupling of light from OLEDs. *Opt. Express* **2011**, *19*, A1272−A1280.
(28) Lim, B. W.; Suh, M. C. Simple fabrication of a three-dimensional porous polymer film as a diffuser for organic light emitting diodes. *Nanoscale* **2014**, *6*, 14446−14452.
(29) Strey, R. Microemulsion microstructure and interfacial curvature. *Colloid Polym. Sci.* **1994**, *272*, 1005−1019.
(30) Reuvers, A. J.; van den Berg, J. W. A.; Smolders, C. A. Formation of membranes by means of immersion precipitation: Part I. A model to describe mass transfer during immersion precipitation. *J. Membr. Sci.* **1987**, *34*, 45−65.
(31) Smolders, C. A.; Reuvers, A. J.; Boom, R. M.; Wienk, I. M. Microstructures in phase-inversion membranes. Part 1. Formation of macrovoids. *J. Membr. Sci.* **1992**, *73*, 259−275.
(32) Kim, S.; Jang, K.-S.; Choi, H.-D.; Choi, S.-H.; Kwon, S.-J.; Kim, I.-D.; Lim, J. A.; Hong, J.-M. Porous Polyimide Membranes Prepared by Wet Phase Inversion for Use in Low Dielectric Applications. *Int. J. Mol. Sci.* **2013**, *14*, 8698−8707.
(33) Wang, H.; Wang, T.; Yang, S.; Fan, L. Preparation of thermal stable porous polyimide membranes by phase inversion process for lithium-ion battery. *Polymer* **2013**, *54*, 6339−6348.
(34) Kim, J. H.; Min, B. R.; Park, H. C.; Won, J.; Kang, Y. S. Phase behavior and morphological studies of polyimide/PVP/solvent/water systems by phase inversion. *J. Appl. Polym. Sci.* **2001**, *81*, 3481−3488.
(35) Bulović, V.; Khalfin, V. B.; Gu, G.; Burrows, P. E.; Garbuzov, D. Z.; Forrest, S. R. Weak microcavity effects in organic light-emitting devices. *Phys. Rev. B: Condens. Matter Mater. Phys.* **1998**, *58*, 3730−3740.
(36) Reineke, S.; Lindner, F.; Schwartz, G.; Seidler, N.; Walzer, K.; Lüssem, B.; Leo, K. White organic light-emitting diodes with fluorescent tube efficiency. *Nature* **2009**, *459*, 234−238.

DOI: 10.1021/acsphotonics.5b00346
ACS Photonics 2015, 2, 1366−1372